ISSN 1812-0512 (Print) 2790-346X (online)

Wasit Journal for Human Sciences

Available online at: https://wjfh.uowasit.edu.iq

Evaluating the Accuracy of Fused OLI Images for Land Cover Classification: A Case Study of Al-Kut City

Rahim Aidan Fadhil Al-Atafi

University of Sumar/ College of Computer and Information Technology

A B S T R A C T

Data fusion is a key technique in remote sensing, enabling the integration of multisensory data to produce more accurate and comprehensive representations of the Earth's surface. Pan-sharpening, particularly the Gram–Schmidt (GS) method, enhances the spatial resolution of multispectral imagery while maintaining spectral fidelity, making it well-suited for Landsat 8 OLI data. This study evaluates the effectiveness of GS pan-sharpening in improving land-cover classification for Kut city, Iraq. Maximum Likelihood Classification (MLC) was adopted as the primary supervised approach, with regions of interest (ROIs) carefully selected and refined through post-classification analysis. Accuracy assessment using confusion matrices showed overall accuracies of 89.35% for 30 m imagery and 78.99% for 15 m imagery, supported by high Kappa coefficients. The results highlight the advantages of integrating GS pan-sharpening with MLC, offering a reliable framework for land-cover mapping and supporting applications in agriculture, environmental monitoring, and urban planning.

***Correspondence*:**
raheemedan@uos.edu.iq

Received: 27 **July** 2025
Accepted: 22 **August** 2025
Published: 01 November 2025

***DOI*:**
https://doi.org/10.31185/wjfh.Vol21.Iss4.1230

***Cite*:**
Al-Atafi , R. A. F. (n.d.). Evaluating the Accuracy of Fused OLI Images for Land Cover Classification: A Case Study of Al-Kut City. Wasit Journal for Human Sciences, 21(4). https://doi.org/10.31185/wjfh.Vol21.Iss4.1230

Keywords: data fusion, Gram-Schmidt, Landsat data 8, Classification, Maximum Likelihood

تقييم دقة الصور المدمجة من مستشعر OLI في تصنيف الغطاء الأرضي:
دراسة حالة مدينة الكوت

د.م. رحيم عيدان فضيل العطافي
جامعة سومر، كلية الحاسوب وتكنولوجيا المعلومات

المُستخلص

تُعدّ دمج البيانات (Data Fusion) تقنيةً أساسيةً في الاستشعار عن بُعد، حيث تتيح تكامل البيانات متعددة الحواس لإنتاج تمثيلات أكثر دقة وشمولية لسطح الأرض. يُعزّز تفعيل حدة الصور البانكروماتية (Pan–sharpening)، وخصوصًا طريقة غرام–شميدت (Gram–Schmidt, GS)، الدقة المكانية للصور متعددة الأطياف مع الحفاظ على الأمان الطيفي، مما يجعلها مناسبة بشكل خاص لبيانات جهاز التصوير التشغيلي الأرضي (OLI) في لاندسات 8. تهدف هذه الدراسة إلى تقييم فعالية طريقة (GS Pan–sharpening)في تحسين تصنيف استخدامات الأراضي لمدينة الكوت في العراق. تم اعتماد طريقة التصنيف بالاحتمال الأقصى(Maximum Likelihood Classification, MLC) كنهج إشرافي رئيسي، مع اختيار مناطق الاهتمام (ROIs) بعناية وتنقيحها من خلال تحليل ما بعد التصنيف. أظهرت تقييمات الدقة باستخدام مصفوفات الالتباس (confusion matrices) دقة إجمالية بلغت 89.35٪ للصور بدقة 30 متر و78.99٪ للصور بدقة 15 متر، مدعومة بمعاملات كابا (Kappa) مرتفعة. تُبرز النتائج مزايا دمج طريقة (GS Pan–sharpening) مع (MLC)، مقدمةً أداة موثوقة.

الكلمات المفتاحية: دمج البيانات، غرام–شميدت، بيانات لاندسات 8، التصنيف، الاحتمالية العظمى

INTRODUCTION

Data fusion integrates information from multiple sensors and databases to deliver more accurate, reliable, and comprehensive representations of the Earth's surface than any single sensor can provide (Ounoughi et al, 2023). Depending on the stage of integration, fusion is often categorized into low-, intermediate-, and high-level strategies. Low-level fusion combines raw measurements, intermediate-level fusion merges features, and high-level fusion aggregates decisions (Kibrete, Woldemichael, & Gebremedhin, 2024). Remote sensing is a prime application domain, where combining heterogeneous sources—optical, thermal, radar, and spectrographic—can offset the limitations of individual sensors and improve downstream tasks such as land-cover mapping and change detection (Segreto et al, 2023).

Within remote sensing, a central stream of fusion research is pan-sharpening, which enhances the spatial resolution of multispectral (MS) imagery by injecting detail from a higher-resolution panchromatic (PAN) band while preserving spectral fidelity. Classical approaches include component-substitution methods such as Intensity–Hue–Saturation (IHS) and Principal Component Analysis (PCA), which substitute a luminance or principal component with the PAN band to transfer spatial detail (Chavez, et al, 1991; Vrabel, 1996). Ratio-based schemes like the Brovey transform normalize MS bands before re-scaling with PAN to emphasize edges and high-frequency structures (Vrabel, 1996). Multiresolution methods (e.g., à trous wavelets, Laplacian pyramids, ARSIS/MTF-based) inject band-limited spatial details extracted from PAN into MS bands to better control spectral distortions (Núñez et al., 1999; Aiazzi, Alparone, Baronti, & Garzelli, 2006). More recently, statistical/Bayesian formulations and learning-based models aim to jointly model spectral–spatial consistency, but they typically demand tuning data or training samples and can be computationally intensive (Vivone et al., 2015).

Among component-substitution techniques, the Gram–Schmidt (GS) method has gained traction due to its simplicity, sensor-agnostic formulation, and favorable balance between spatial enhancement and spectral preservation. GS constructs a synthetic PAN from the MS bands, orthogonalizes the spectral space via a Gram–Schmidt transform, and then replaces the first component with the true PAN before inverting the transform (Laben et al, 2000). This procedure reduces color (hue) shifts common in naïve substitutions by better aligning the injected spatial detail with the MS spectral subspace (Pohl et al, 2014; Vivone et al., 2015). Given the characteristics of Landsat OLI—moderate-resolution MS bands complemented by a higher-resolution PAN band (Band 8)—GS pan-sharpening is a strong candidate to raise classification performance where fine spatial structures (field boundaries, urban edges) matter.

In practical workflows, the value of pan-sharpening is ultimately judged by downstream utility, not only by spectral/spatial quality indices. While quantitative image-quality metrics (e.g., SAM, ERGAS, QNR) are informative, gains must translate into higher thematic accuracy in supervised classification pipelines relevant to agriculture, environmental monitoring, and urban studies (Vivone et al., 2015; Pohl & Van Genderen, 2014). This study, therefore, emphasizes end-task performance on OLI imagery.

Research problem: single-sensor OLI multispectral data at native resolution often yield suboptimal land-cover discrimination in heterogeneous landscapes where classes share overlapping spectral signatures, and existing pan-sharpening approaches can introduce spectral distortions that degrade thematic accuracy.

Research objective: to evaluate whether Gram–Schmidt pan-sharpening of Landsat OLI imagery improves supervised land-cover classification accuracy compared with unsharpened MS data.

Practical significance: demonstrating a reliable accuracy gain would support operational mapping in precision agriculture (field-scale crop monitoring), environmental management (land-cover/land-use inventories), and urban planning (detailed land-use delineation), informing cost-effective workflows that leverage freely available Landsat data.

MATERIALS AND METHODS

Study area

The administrative center and capital of Wasit Governorate in eastern Iraq is situated between 32°00′N–33°00′N latitude and 45°00′E–47°00′E longitude (Mohsin et al., 2014) (Figure 1). It lies on the Tigris River, at approximate central coordinates of 32.5°N and 45.8°E, about 180 km southeast of Baghdad. The city is surrounded by water on several sides, as the Tigris is joined by the Gharaf and Dijail Rivers, which provide abundant water resources and enhance the fertility of its agricultural lands (Muslim et al., 2019). Wasit Governorate, with a total area of about 17,153 km² (nearly 4% of Iraq's 441,000 km²), is bordered by Baghdad to the north, Maysan to the south, Qadisiya to the west, and Iran to the east. Covering approximately 1,514 km², this urban center plays a vital role in the province's economy (Hamoodi, 2023). It is well known for its agricultural production, particularly wheat, barley, sesame, dates, and vegetables, as well as its rich fish resources. Moreover, its strategic location strengthens its economic and commercial importance by linking Iraq internally and with neighboring countries, especially Iran(Jasim et al., 2021). As of 2024, the population is estimated at around 512,000 inhabitants, with continuous annual growth, underscoring its significance as both an agricultural and commercial hub(Al-Zuhairy et al., 2024).

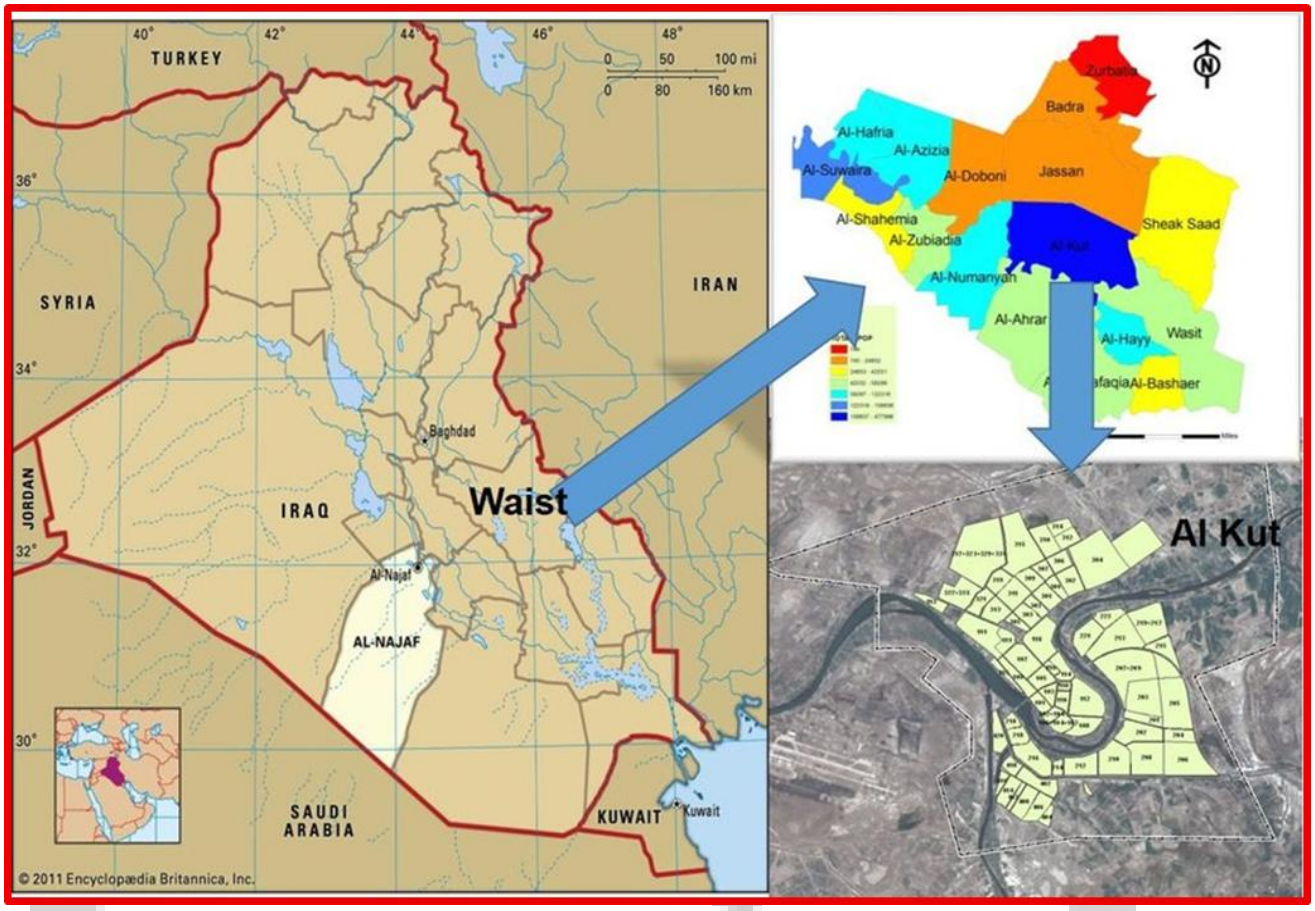

Figure 1. Location map of the study area (Kut city within Wasit Province, Iraq).

Datasets

Data Fusion Approach

Data fusion integrates information from multiple sensors to improve analysis and decision-making across various fields(Xue et al., 2017). In defense, it enhances Reconnaissance, Surveillance, Target Acquisition, and Kill Assessment (RSTAKA) operations. In industrial and environmental applications, it synchronizes sensor inputs to monitor production processes or track the dispersion of pollutants. In medicine, it supports diagnosis and patient monitoring through diverse sensors, and in transportation, it enables intelligent vehicles and smart highways (Jain et al., 2023).

The process employs methods such as statistical classification, feature analysis, and neural networks. Statistical classification identifies patterns in data, feature analysis matches specific target characteristics, and neural networks detect complex patterns(Gong et al., 2024). Unlike single-sensor operations, data fusion combines patterns from multiple sources using approaches like Bayesian analysis, Dempster–Shafer theory, or voting. Feature-level fusion generally yields superior results, especially when characteristics are independent (Zhao et al., 2024).

Landsat 8 and Remote Sensing Applications

Landsat 8, launched on February 11, 2013, from Vandenberg Air Force Base, California, aboard an Atlas-V 401 rocket, is a key satellite in NASA's Landsat program for Earth observation Table 1 (Wu et al., 2024). It carries the **Operational Land Imager (OLI)** and **Thermal Infrared Sensor (TIRS)**, capturing multiple spectral bands at 15 m (panchromatic), 30 m (visible, NIR, SWIR), and 100 m (thermal), enabling the integration of spectral and spatial data for improved environmental monitoring and land-use analysis (Singh et al., 2024).

Developed collaboratively by NASA and the U.S. Geological Survey (USGS), the satellite was initially designated the **Landsat Data Continuity Mission (LDCM)** and was renamed **Landsat 8** upon entering routine operations. NASA managed design, launch, and calibration, while USGS oversees post-launch operations, data processing, and archiving (Wang et al., 2024).

Table (1): Representation of Landsat 8

Information	Band	Wavelength (micrometers)	Resolution (meters)
Landsat 8	Band 1 - coastal aerosol	0.43 ˜ 0.45	30
Operational	Band 2 - Blue	0.45 ˜ 0.51	30
Landsat Image	Band 3 - Green	0.53 ˜ 0.59	30
(OLI)	Band 4 - Red	0.64 ˜ 0.67	30
and	Band 5 - Near Infrared (NIR)	0.85 ˜ 0.88	30
Thermal	Band 6 - SWIR 1	1.57 ˜ 1.65	30
Infrared	Band 7 - SWIR 2	2.11 ˜ 2.29	30
sensor	Band 8 - Panchromatic	0.50 ˜ 0.68	15
Launched	Band 9 - Cirrus	1.36 ˜ 1.38	30
February	Band 10 - Thermal IR (TIRS) 1	10.60 ˜ 11.19	100 * 30
11,2013	Band 11 - Thermal IR (TIRS) 2	11.50 ˜ 12.51	100 * 30

Landsat data

Landsat 8 was launched on February 11, 2013, from Vandenberg Air Force Base, California, using an Atlas-V 401 rocket with an extended payload fairing from United Launch Alliance, LLC. The satellite's payload includes the Operational Land Imager and Thermal Infrared Sensor (Wu et al., 2024). The sensors offer seasonal landmass coverage with spatial resolutions of 30 meters (visible, NIR, SWIR), 100 meters (thermal), and 15 meters (panchromatic) (Singh et al., 2024) .

NASA and the U.S. Geological Survey (USGS) collaborated to develop Landsat 8. The satellite was designated as the Landsat Data Continuity Mission (LDCM) during the design, production, launch, and on-orbit calibration stages, which were overseen by NASA (Wang et al., 2024). routine operations, and the satellite was renamed Landsat 8 on May 30, 2013. The United States Geological Survey (USGS) is the dominant entity in the Earth's post-launch calibration, satellite operations, data product generation, and data archiving as viewed in Table 2 below (Mustaquim et al, 2024).

Table 2. Characteristics of the Landsat 8 Operational Land Imager (OLI) and Thermal Infrared Sensor (TIRS) bands [4].

Band	Name	Band Width (λ, µm)	Spatial Resolution
1	Blue	0.45 ˜ 0.515	30 m
2	Green	0.525 ˜ 0.605	30 m
3	Red	0.63 ˜ 0.69	30 m
4	Near Infrared	0.75 ˜ 0.90	30 m
5	Shortwave IR 1	1.55 ˜ 1.75	30 m
6	Thermal IR	10.4 ˜ 12.5	60 m / 120 m
7	Shortwave IR 2	2.09 ˜ 2.35	30 m
8	Panchromatic	0.52 ˜ 0.9	15 m

Evolutionary Advances

The instruments onboard Landsat 8 represent a significant evolutionary advance in satellite observation technology (Williams, et al, 2024). The Operational Land Imager (OLI) builds upon previous Landsat sensors by adopting a technological approach initially demonstrated by the sensor aboard NASA’s experimental EO-1 satellite (Elshewy, et al, 2024; Yarahmadi et al., 2024).

The OLI instrument was designed with an expected operational lifetime of five years. Compared to the Enhanced Thematic Mapper Plus (ETM+) on Landsat 7, OLI introduces two additional spectral bands specifically designed for cirrus cloud detection and coastal/aerosol observations (Badapalli, et al, 2025).

Landsat 8 Mission Objectives

The primary objective of the **Landsat 8 mission** is to provide periodic, high-quality visible and infrared imagery covering the Earth's landmasses and near-coastal regions, while continuously updating and maintaining the existing Landsat database (Levy et al, 2024).

The consistency between newly acquired data and the archived records—particularly with respect to acquisition geometry, calibration, coverage, and spectral properties—ensures the reliability of global and regional change detection, as well as accurate characterization of environmental information (Mamun, et al, 2024).

Gram–Schmidt Process

A well-known method for building orthonormal bases is the Gram–Schmidt process. It converts a set of linearly independent real functions into an orthonormal set with respect to a defined weighting function, ensuring orthogonality within the functional space (Balabanov et al, 2025).

In remote sensing, the Gram–Schmidt Spectral Sharpening (GS) method is applied to improve wavelength discrimination across multiple spectral bands(Balabanov & Grigori, 2025).

This enhancement is achieved by integrating high–spatial–resolution data, which strengthens both spectral and spatial information(Chen, 2025).

Classification

Remotely sensed data can be classified into distinct categories based on the homogeneity of pixel characteristics, which enables the differentiation of multiple land-cover types within an image (Berlin, 2024). Classification is considered one of the fundamental techniques in remote sensing, as it relies on taxonomic criteria that facilitate satellite data analysis and the generation of thematic maps (Cheong & Huang, 2025).

In the present study, classification was applied following the identification of regions of interest (ROI), including water, soil, built-up areas, and vegetation(Berlin, 2024). These ROIs were used as training samples to represent the spectral signatures of each class(Alnuaimi & Albaldawi, 2024). Digital image processing software was employed to compute the brightness values of image elements, which were then classified according to predefined criteria.

The Maximum Likelihood Classification (MLC) method was adopted, as it assumes that the statistics for each class in each band are normally distributed and assigns each pixel to the class with the highest probability(Jasim, 2025). This approach is widely recognized for producing higher accuracy compared with other parametric classifiers. After the initial classification, a post-classification refinement was conducted to further assess the accuracy(Chowdhury, 2024). The classified ROIs were compared with the original training sites using a confusion matrix, and ground truth data were employed to validate the results and evaluate the reliability of the land-cover maps(Libal & Biernacki, 2024).

Although alternative machine learning classifiers such as Support Vector Machine (SVM) and Random Forest (RF) have gained popularity due to their ability to handle non-linear class boundaries and complex feature spaces, MLC remains a reliable choice in cases where training data are limited and the underlying class distributions are approximately normal(Parkinson et al., 2024). SVM often requires careful kernel selection and parameter tuning, while RF depends on large training datasets to achieve stable results. In contrast, MLC provides a balance between computational efficiency and classification accuracy, making it particularly suitable for medium-resolution datasets such as Landsat OLI. This justifies its selection as the primary classification approach in the present study(Wen et al., 2024).

RESULTS

Classification 30 m

To obtain accurate data for the classification process, a training aerial photograph of the city of Kut was utilized Figure 2. The dataset included images with spatial resolutions of 30 m and 15 m, which provided sufficient detail for selecting representative training areas. The classification process required the careful identification of training sites to serve as the basis for assigning pixels to specific land-cover classes. Subsequent comparison and estimation procedures were then applied to determine the likelihood of each pixel belonging to a given class.

The procedure consisted of the following steps as shown in chart 1:

1. Image Preparation: An aerial view of the city of Kut with a spatial resolution of 30 m was opened and prepared for analysis.
2. Selection of Training Areas (ROIs): Regions of interest (ROIs) were identified to represent the major land-cover classes, including water, soil, built-up areas, and vegetation. These ROIs served as training sets to characterize the spectral signatures of each class.

3. Classification: The Maximum Likelihood Classification (MLC) method was applied. This approach evaluates the probability distribution of spectral values for each class and assigns pixels to the class with the highest probability. The training areas were used as the foundation for classification, ensuring that each pixel was categorized according to its similarity to the spectral characteristics of the predefined classes.

4. Post-Classification Analysis: Following the initial classification, a post-classification refinement was carried out using ground-truth ROIs. A confusion matrix was generated to compare the classified results with reference data, thereby assessing accuracy. This process produced a thematic report distinguishing the main land-cover categories of the study area, as presented in Table 3، namely water, soil, vegetation, and built-up surfaces.

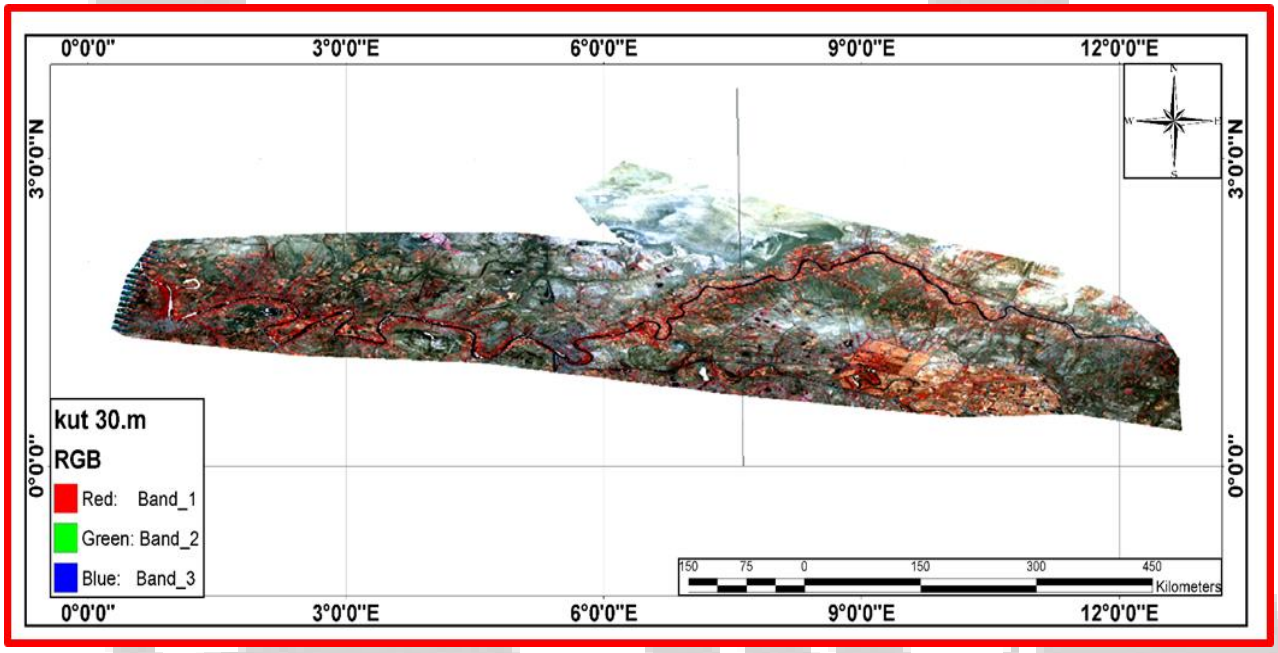

Figure 2: Aerial Image of Kut City at 30 m Resolution

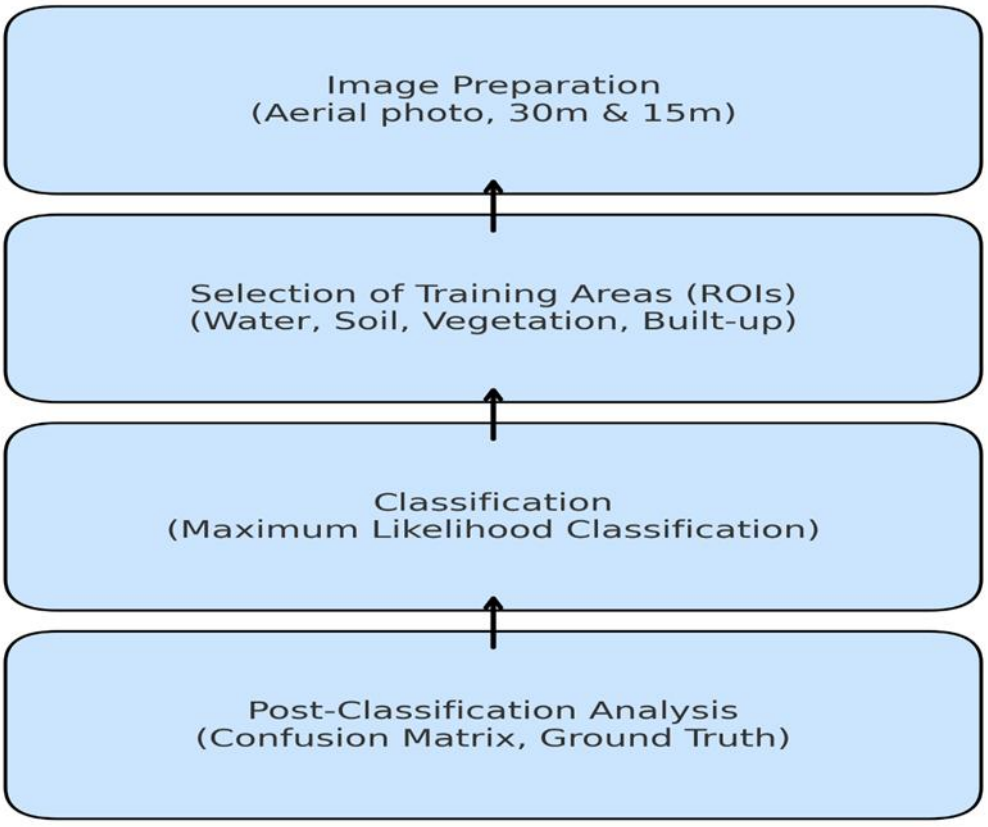

Chart 1: Workflow of Land-Cover Classification Using Aerial Imagery of Kut City

Table 3. displays the kappa coefficient, confusion matrix, producer accuracy 30M, errors of commission, and errors of omission.

Overall accuracy = (1946/2178) 89.3480%
Kappa Coefficient = 0.8558

Ground Truth (Pixels)

Class	water test	soil test	build test	vegetation test	Total
Unclassified	8	0	0	0	8
Water [Blue]	390	0	0	0	390
Soil [Red] 89	0	491	0	0	491
Build [Yellow	0	1	424	0	425
Vegetation [G	1	218	4	641	864
Total	399	710	428	641	2178

Ground Truth (Percent)

Class	water test	soil test	build test	vegetation test	Total
Unclassified	2.01	0.00	0.00	0.00	0.37
Water [Blue]	97.74	0.00	0.00	0.00	17.91
Soil [Red] 89	0.00	69.15	0.00	0.00	22.54
Build [Yellow	0.00	0.14	99.07	0.00	19.51
Vegetation [G	0.25	30.70	0.93	100.00	39.67
Total	100.00	100.00	100.00	100.00	100.00

Class	Commission (Percent)	Omission (Percent)	Commission (Pixels)	Omission (Pixels)
Water [Blue]	0.00	2.26	0/390	9/399
Soil [Red] 89	0.00	30.85	0/491	219/710
Build [Yellow	0.24	0.93	1/425	4/428
Vegetation [G	25.81	0.00	223/864	0/641

Class	Prod. Acc. (Percent)	User Acc. (Percent)	Prod. Acc. (Pixels)	User Acc. (Pixels)
Water [Blue]	97.74	100.00	390/399	390/390
Soil [Red] 89	69.15	100.00	491/710	491/491
Build [Yellow	99.07	99.76	424/428	424/425
Vegetation [G	100.00	74.19	641/641	641/864

The classification results of the study demonstrated a high overall accuracy of 89.35%, with a corresponding Kappa coefficient of 0.856, indicating strong agreement between the classified image and ground truth data. The analysis considered four land-cover classes: water, soil, vegetation, and built-up areas.

- Water: Out of a total of 399 pixels representing water, 390 pixels were correctly classified. Eight pixels were unclassified, and one pixel was misclassified as vegetation.
- Soil: The total number of soil pixels was 710. While this number was correctly identified, 218 pixels were incorrectly classified as vegetation, and one pixel was misclassified as built-up.
- Built-up Areas: Among 428 pixels representing construction, all were correctly identified; however, 424 pixels were erroneously classified as vegetation.
- Vegetation: A total of 641 pixels representing vegetation were correctly classified, reflecting the highest accuracy among the classes.

Omission error for each class was calculated as the percentage of pixels that were incorrectly omitted from their true class. The commission error was determined by calculating the proportion of pixels assigned incorrectly to a class relative to the total pixels classified as that class. These error metrics

provide a quantitative assessment of the misclassification patterns, highlighting which classes were overrepresented or underrepresented in the classified map.

Overall, the high accuracy and Kappa coefficient indicate that the applied Maximum Likelihood Classification (MLC), combined with carefully selected training ROIs, was effective in producing reliable land-cover maps for the study area.

Where:

	Omission	commission	mapping accuracy
Water	$\frac{9}{399} = 2.2$	$\frac{381}{399} = 95.48$	$\frac{390}{390+9+381} = 50\%$
Soil	$\frac{219}{710} = 30.85$	$\frac{272}{710} = 38.30$	$\frac{491}{491+219+272} = 50\%$
Build	$\frac{4}{428} = 0.24$	$\frac{400}{428} = 90.89$	$\frac{424}{424+4+400} = 51\%$
Vegetation	$\frac{0}{641} = 0.00$	$\frac{641}{641} = 10.00$	$\frac{641}{641+0+641} = 50\%$

Overall Landsat classification accuracy = $\frac{390+491+424+641}{2178} = 89.34\%$

In this study, both unsupervised and supervised classification methods were applied, with a primary focus on the Maximum Likelihood Classification (MLC) due to its effectiveness in handling high-resolution imagery. Following classification, **a** post-classification refinement was conducted, and the results were evaluated using **a** confusion matrix. Both 30 m and 15 m resolution aerial images of the city of Kut were analyzed, with MLC chosen for its superior performance in high spatial resolution data compared to alternative classification approaches.

Regions of interest (ROI**s**) were carefully selected for the 30 m aerial imagery, representing key land-cover classes such as water, soil, vegetation, and built-up areas. These ROIs were compared with post-classification ROIs to assess the classification accuracy. The overall accuracy achieved in the selection and classification of training areas was 89.34%**,** with a corresponding Kappa coefficient of 0.85, indicating strong agreement between the classified image and ground truth data, as noted in Figure 3.

The error analysis revealed variability across classes. The built-up areas exhibited the lowest error rate, with only 4 pixels misclassified as vegetation. In contrast, the soil class showed the highest error rate, with 218 pixels incorrectly classified, highlighting the relative difficulty in distinguishing soil from other land-cover types in this study area.

These results demonstrate that the combination of careful ROI selection, Maximum Likelihood Classification, and post-classification refinement can produce highly accurate land-cover maps for both

medium- and high-resolution aerial imagery, while also identifying classes that may require further attention in future analyses.

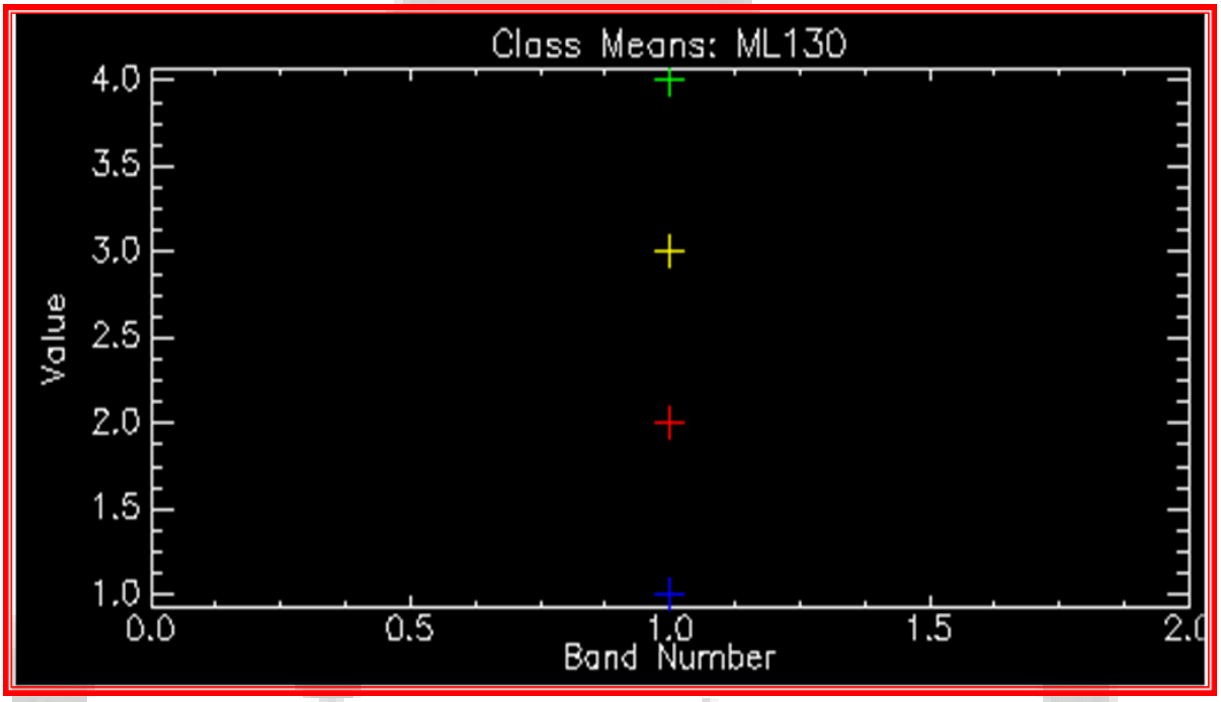

Figure 3: Histogram Representing Class Distribution for 30 m Imagery

Classification 15 m

Use the same steps are followed in the picture 30 m, and the addition of the image data and the identification of training by (ROI), and classification's then report on the 15 m. As presented in Figure 4 and Table 4

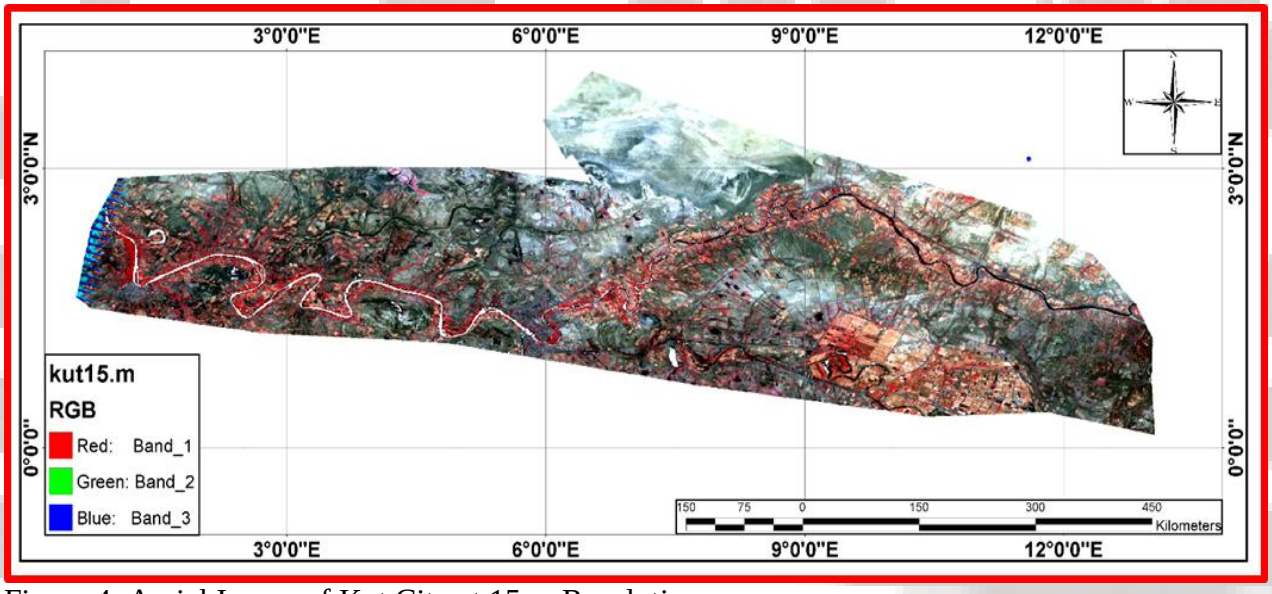

Figure 4: Aerial Image of Kut City at 15 m Resolution

Table 4. displays the kappa coefficient, confusion matrix, producer accuracy 15M, errors of commission, and errors of omission.

Overall accuracy = (2768/3504) 78.9954%
Kappa Coefficient = 0.7168

Ground Truth (Pixels)

Class	water test	soil test	build test	vegetation test	Total
Unclassified	78	0	0	1	79
Water [Blue]	789	0	0	0	789
Soil [Red] 91	0	1028	6	0	1034
Build [Yellow	0	650	448	0	1098
Vegetation [G	1	0	0	503	504
Total	868	1678	454	504	3504

Ground Truth (Percent)

Class	water test	soil test	build test	vegetation test	Total
Unclassified	8.99	0.00	0.00	0.20	2.25
Water [Blue]	90.90	0.00	0.00	0.00	22.52
Soil [Red] 91	0.00	61.26	1.32	0.00	29.51
Build [Yellow	0.00	38.74	98.68	0.00	31.34
Vegetation [G	0.12	0.00	0.00	99.80	14.38
Total	100.00	100.00	100.00	100.00	100.00

Class	Commission (Percent)	Omission (Percent)	Commission (Pixels)	Omission (Pixels)
Water [Blue]	0.00	9.10	0/789	79/868
Soil [Red] 91	0.58	38.74	6/1034	650/1678
Build [Yellow	59.20	1.32	650/1098	6/454
Vegetation [G	0.20	0.20	1/504	1/504

Class	Prod. Acc. (Percent)	User Acc. (Percent)	Prod. Acc. (Pixels)	User Acc. (Pixels)
Water [Blue]	90.90	100.00	789/868	789/789
Soil [Red] 91	61.26	99.42	1028/1678	1028/1034
Build [Yellow	98.68	40.80	448/454	448/1098
Vegetation [G	99.80	99.80	503/504	503/504

Report shows that the overall accuracy of the classification was high as the percentage (78.9954%) The Kappa coefficient was (0.7168 %)

Omission: is obtained by dividing the entire number of pixels in 100, which is incorrect.

Where:

	Omission	commission	mapping accuracy
Water	$\frac{79}{868} = 9.10$	$\frac{710}{868} = 81.79$	$\frac{789}{789+79+710} = 50\%$
Soil	$\frac{650}{1678} = 38.74$	$\frac{378}{1678} = 22.52$	$\frac{1028}{1028+650+378} = 50\%$
Build	$\frac{6}{454} = 1.32$	$\frac{442}{454} = 97.35$	$\frac{448}{448+6+442} = 50\%$
Vegetation	$\frac{1}{504} = 0.20$	$\frac{502}{504} = 99.60$	$\frac{503}{503+1+502} = 50\%$

Overall Landsat classification accuracy = $\frac{789+1028+448+503}{3504} = 78.99\%$

In this study, regions of interest (**ROIs**) were identified on the 15 m aerial imagery of the city of Kut and compared with the results of **post-classification refinement**. The overall classification accuracy for the selection of ROIs was relatively lower than that of the 30 m imagery, achieving **78.99%,** with a corresponding **Kappa coefficient of 0.71**, indicating moderate agreement between the classified image and the **reference data, as shown in Figure 5**.

The **error analysis** revealed variability across different land-cover classes. The vegetation class exhibited the **lowest error rate**, with only **one pixel misclassified**, demonstrating high reliability for this category. In contrast, the soil class showed the **highest error rate,** with **650 pixels incorrectly classified as built-up areas**, highlighting the challenge of distinguishing soil from construction in the study area.

The **omission and commission errors** were consistent with the ROI-based accuracy assessment. These metrics confirmed that the classification patterns observed for the 15 m imagery were in line with those identified in the 30 m dataset, validating the reliability of the methodology across multiple spatial resolutions.

Overall, despite the slightly lower accuracy at 15 m resolution, the combination of careful ROI selection, Maximum Likelihood Classification, and post-classification analysis provided a **robust framework for land-cover mapping** of Kut city.

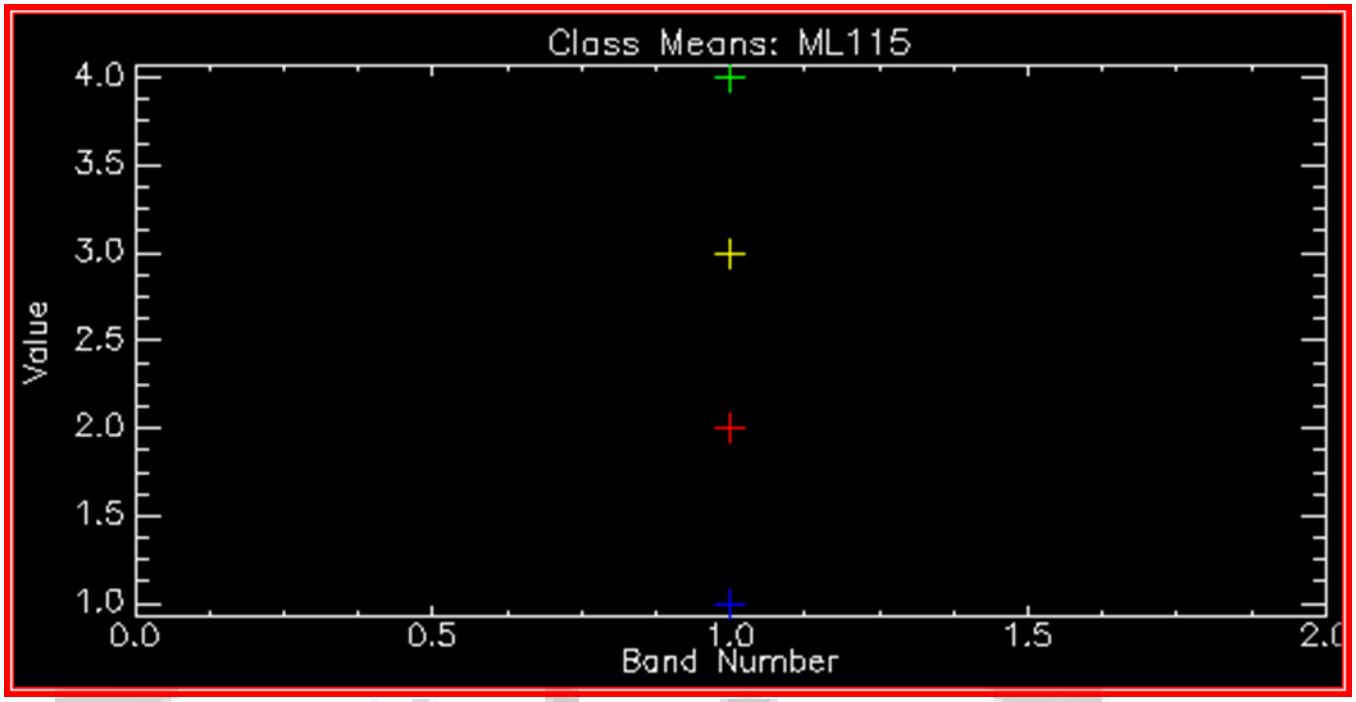

Figure 5: Histogram Representing Class Distribution for 15 m Imagery

CONCLUSIONS

1. Schmidt (GS) pan-sharpening method in enhancing the classification accuracy of Landsat OLI imagery for the city of Kut. The research demonstrated that the data fusion process was effective in improving the selection of regions of interest (ROIs) for supervised classification and post-classification analysis.
2. The study followed a structured workflow: the 30 m original imagery of Kut was first analyzed, followed by the 15 m Gram–Schmidt pan-sharpened imagery. Data fusion was applied to enhance the spatial resolution while preserving spectral information, which facilitated the accurate selection of training ROIs for both images. The overall classification accuracy achieved was 89.35% for the 30 m image and 78.99% for the 15 m image, with corresponding Kappa coefficients of 0.856 and 0.71, respectively. These results indicate that the GS method significantly improves classification reliability compared to unsharpened images, particularly in heterogeneous urban and peri-urban landscapes.
3. Maximum Likelihood Classification (MLC) was employed as the primary supervised classification approach due to its effectiveness with high spatial resolution imagery. Post-classification refinement and confusion matrix analysis confirmed the robustness of the methodology, showing minimal omission and commission errors for most classes, with the exception of soil and built-up areas, which exhibited higher misclassification rates in the 15 m imagery.
4. The Gram–Schmidt transform provided two major advantages:

• Enhanced spatial resolution of multispectral imagery, allowing better discrimination of land-cover classes.
• Preservation of spectral integrity, reducing distortions common in other fusion-based methods.

5. Additional insights from the study include:

• Vegetation and water classes were consistently classified with high accuracy in both resolutions, demonstrating the reliability of training ROI selection.
• Soil and built-up areas showed higher error rates at 15 m resolution, suggesting that finer spatial resolution improves the discrimination of spectrally similar classes.

• Data fusion combined with careful ROI selection reduces errors in supervised classification, supporting its use in operational land-cover mapping and urban planning applications.

6. In conclusion, the integration of Gram–Schmidt pan-sharpening with Maximum Likelihood Classification provides a robust and accurate framework for land-cover mapping using medium- and high-resolution satellite imagery. This approach is recommended for future studies requiring precise classification in complex urban and heterogeneous landscapes.

REFERENCES

Aiazzi, B., Alparone, L., Baronti, S., & Garzelli, A. (2006). MTF-based spectral distortion minimization in pan-sharpening of very high resolution multispectral images. IEEE Transactions on Geoscience and Remote Sensing, 44(10), 3168–3179.

Chavez, P. S., Sides, S. C., & Anderson, J. A. (1991). Comparison of three different methods to merge multiresolution and multispectral data: TM & SPOT Panchromatic. Photogrammetric Engineering & Remote Sensing, 57(3), 295–303.

Kibrete, F., Woldemichael, A., & Gebremedhen, A. (2024). A review of data fusion levels and applications. Journal of Imaging and Geoinformation, 12(1), 45–62.

Laben, C. A., & Brower, B. V. (2000). Process for enhancing the spatial resolution of multispectral imagery using pan-sharpening (U.S. Patent No. 6,011,875).

Núñez, J., Otazu, X., Fors, O., Prades, A., Pala, V., & Arbiol, R. (1999). Multiresolution-based image fusion with additive wavelet decomposition. IEEE Transactions on Geoscience and Remote Sensing, 37(3), 1204–1211.

Ounoughi, N., & Yahia, S. B. (2023). Data fusion: Concepts, models, and applications. Information Fusion Letters, 5(2), 1–15.

Pohl, C., & Van Genderen, J. (2014). Multisensor image fusion in remote sensing (2nd ed.). CRC Press.

Segreto, V., & Teti, R. (2023). Heterogeneous Sensor Fusion: Opportunities and Challenges. Sensors, 23(15), 6789.

Vivone, G., et al. (2015). A critical comparison among pansharpening algorithms. IEEE Transactions on Geoscience and Remote Sensing, 53(5), 2565–2586.

Vrabel, J. (1996). Multispectral imagery band sharpening study. Photogrammetric Engineering & Remote Sensing, 62(9), 1075–1083.

Al-Zuhairy, M. S., Wadeea, S. I., & Hamdoon, R. M. (2024). Water pollution utilizing the relative weight water quality index with geographic information system for Tigris river at Wassit. AIP Conference Proceedings,

Alnuaimi, A. F., & Albaldawi, T. H. (2024). An overview of machine learning classification techniques. BIO Web of Conferences,

Balabanov, O., & Grigori, L. (2025). Randomized block Gram–Schmidt process for the solution of linear systems and eigenvalue problems. *SIAM Journal on Scientific Computing*, *47*(1), A553-A585.

Berlin, B. (2024). Ethnobiological classification. In *Cognition and categorization* (pp. 9-26). Routledge.

Chen, R.-M. (2025). A Non-Self-Referential Characterization of the Gram–Schmidt Process via Computational Induction. *Mathematics (2227-7390), 13*(5).

Chowdhury, M. S. (2024). Comparison of accuracy and reliability of random forest, support vector machine, artificial neural network and maximum likelihood method in land use/cover classification of urban setting. *Environmental Challenges*, *14*, 100800.

Gong, Y., El-Monier, I., & Mehana, M. (2024). Machine learning and data fusion approach for elastic rock properties estimation and fracturability evaluation. *Energy and AI*, *16*, 100335.

Jasim, A. T. (2025). Assessing LULC dynamics in Kirkuk City, Iraq using Landsat imagery and maximum likelihood classification. *DYSONA-Applied Science*, *6*(1), 113-119.

Jasim, I. A., Mahmood, T. S., Al-Mamoori, S. K., & Al-Maliki, L. A. (2021). The relationship between traffic congestion and land uses: A case study of Al-Kut city, Iraq. *Journal of Urban Regeneration & Renewal*, *14*(3), 264-271.

Libal, U., & Biernacki, P. (2024). Non-intrusive system for honeybee recognition based on audio signals and maximum likelihood classification by autoencoder. *Sensors*, *24*(16), 5389.

Parkinson, F., Douglas, K., Li, Z., Meijer, A., Stacey, C. D., Kung, R., & Podhorodeski, A. (2024). A Generalized Semiautomated Method for Seabed Geology Classification Using Multibeam Data and Maximum Likelihood Classification. *Journal of Coastal Research*, *40*(1), 1-16.

Singh, G., Dahiya, N., Sood, V., Singh, S., Sharma, A. J. E. M., & Assessment. (2024). ENVINet5 deep learning change detection framework for the estimation of agriculture variations during 2012–2023 with Landsat series data. *196*(3), 233.

Wen, L., Chen, S., Hong, Z., & Zheng, L. (2024). Maximum likelihood weight estimation for partial domain adaptation. *Information Sciences*, *676*, 120800.

Wu, H., Liu, Y., Pu, Y., Liu, P., Zhao, W., Guo, X. J. I. J. o. P., & Sensing, R. (2024). National-scale nighttime high-temperature anomalies from Landsat-8 OLI images. *212*, 212-229.

Xue, J., Leung, Y., & Fung, T. (2017). A Bayesian data fusion approach to spatio-temporal fusion of remotely sensed images. *Remote Sensing*, *9*(12), 1310.